Energy & Environmental Science

PAPER

View Article Online
View Journal | View Issue

Cite this: *Energy Environ. Sci.*, 2019, **12**, 2559

Singlet oxygen from cation driven superoxide disproportionation and consequences for aprotic metal–O_2 batteries†

Eléonore Mourad,[a] Yann K. Petit,[a] Riccardo Spezia,[b] Aleksej Samojlov,[a] Francesco F. Summa,[c] Christian Prehal,[a] Christian Leypold,[a] Nika Mahne,[a] Christian Slugovc,[a] Olivier Fontaine,[de] Sergio Brutti*[f] and Stefan A. Freunberger*[a]

Received 6th May 2019,
Accepted 16th July 2019

DOI: 10.1039/c9ee01453e

rsc.li/ees

Aprotic alkali metal–oxygen batteries require reversible formation of metal superoxide or peroxide on cycling. Severe parasitic reactions cause poor rechargeability, efficiency, and cycle life and have been shown to be caused by singlet oxygen ($^1O_2$) that forms at all stages of cycling. However, its formation mechanism remains unclear. We show that disproportionation of superoxide, the product or intermediate on discharge and charge, to peroxide and oxygen is responsible for $^1O_2$ formation. While the overall reaction is driven by the stability of peroxide and thus favored by stronger Lewis acidic cations such as Li^+, the $^1O_2$ fraction is enhanced by weak Lewis acids such as organic cations. Concurrently, the metal peroxide yield drops with increasing $^1O_2$. The results explain a major parasitic pathway during cell cycling and the growing severity in K–, Na–, and Li–O_2 cells based on the growing propensity for disproportionation. High capacities and rates with peroxides are now realized to require solution processes, which form peroxide or release O_2 *via* disproportionation. The results therefore establish the central dilemma that disproportionation is required for high capacity but also responsible for irreversible reactions. Highly reversible cell operation requires hence finding reaction routes that avoid disproportionation.

Broader context

Decarbonizing the energy system requires energy storage with large capacity but equally low economic and ecological footprint. Alkali metal–O_2 batteries are considered outstanding candidates in this respect. However, they suffer from poor cycle life as a result of cathode degradation. Formation of the highly reactive singlet oxygen has been proposed to cause this degradation, but formation mechanisms have remained unclear. Here, we show that the singlet oxygen source is the disproportionation of thermodynamically unstable superoxide intermediates to the peroxides. The revealed mechanism conclusively explains the strongly growing degree of degradation when going from K–O_2 to Na–O_2 and Li–O_2 cells. A major consequence is that highly reversible cell operation of Li–O_2 and Na–O_2 cells requires them to form and decompose the peroxides without disproportionation. Achieving this requires finding new reaction routes. The work lays the mechanistic foundation to fight singlet oxygen as the predominant source of degradation in metal–O_2 cells.

Introduction

Advancing electrochemical storage beyond the limits of current batteries has become the focus of much cutting-edge research and hence has caused immense interest in rechargeable non-aqueous alkali metal–O_2 batteries. They operate by reversibly forming/decomposing superoxides or peroxides of Li, Na, or K at a porous cathode according to

$$O_2 + xe^- + xM^+ \leftrightarrow M_xO_2 \ (M = Li, Na, K) \quad (1)$$

The products that typically form are Li_2O_2, Na_2O_2, NaO_2, or KO_2.[1–5] Practically realizing such cells faces, however, two major barriers. First, these (su)peroxides are insulating solids

[a] *Institute for Chemistry and Technology of Materials, Graz University of Technology, Stremayrgasse 9, Graz 8010, Austria. E-mail: freunberger@tugraz.at*
[b] *Laboratoire de Chimie Théorique, UMR 7616 CNRS, Sorbonne Université, CC 137, 4, Place Jussieu, 75252 Paris Cedex 05, France*
[c] *Dipartimento di Scienze, Università della Basilicata, V.le Ateneo Lucano 10, 85100 Potenza, Italy*
[d] *Institut Charles Gerhardt Montpellier, UMR 5253, CC 1701, Université Montpellier, Place Eugène Bataillon, 34095 Montpellier Cedex 5, France*
[e] *Réseau sur le Stockage Electrochimique de l'Energie (RS2E), CNRS FR3459, 33 rue Saint Leu, 80039 Amiens, France*
[f] *Dipartimento di Chimica, Università di Roma La Sapienza, P.le A. Moro 5, 00185 Roma, Italy. E-mail: sergio.brutti@unibas.it*

† Electronic supplementary information (ESI) available: Supporting methods, figures, tables and notes. See DOI: 10.1039/c9ee01453e

that passivate the electrode and lead to low capacities. Large capacities and high rates are now realized to require solution processes on both discharge and charge, which may be favored by solvating additives or mediators.[2,6–13] Second, severe parasitic reactions decompose the electrolyte and electrode and cause high charging voltage, poor reversibility and cycle life.[1–3,7,14–25]

The parasitic reactions cause deviations from the ideal cell reaction in eqn (1). Key measures for parasitic chemistry are the ratio of O_2 consumed/evolved and peroxide or superoxide formed/decomposed per electron passed on discharge/charge. Parasitic reactions form significant amounts of side products such as alkali carbonate, carboxylates, or CO_2.[2,3,13,15,17,20–22,26,27] The severity of parasitic chemistry increases in the order K–O_2, Na–O_2, and Li–O_2 with typical (su)peroxide yields of ~98–100%, ~90–95%, and 50–90%, respectively, and similar O_2 yields on recharge.[3,5,10,13,15,17,20–22,26–29] Peroxide rather than superoxide as the product increases the severity, particularly on charge, where the voltage climbs inexorably due, in large parts, newly formed parasitic products.[15,17,20–22,25,30,31]

The parasitic reactions have long been predominantly ascribed to the direct reactivity of electrolyte or carbon with superoxides and peroxides owing to their basicitiy, nucleophilicity, or radical nature.[2,3,15,17,19–22,27,28] Nevertheless, these reactivities fail to conclusively explain the mentioned pattern of parasitic reactions. Specifically, the extent of side reactions would suggest the reactivity to seemingly severely grow in the order $KO_2 < NaO_2 < LiO_2$, and superoxides to be less reactive than peroxides, which opposes chemical intuition suggesting KO_2 to be the most reactive. KO_2 can, however, cycle highly reversible as recently shown by Lu *et al.*,[5] which forcefully demonstrates that other degradation pathways than superoxide attack must prevail. Only recently, the highly reactive singlet oxygen ($^1O_2$ or $^1\Delta_g$), the first excited state of ground state triplet oxygen ($^3O_2$ or $^3\Sigma_g^-$), has been revealed to form upon cycling in Li–O_2 and Na–O_2 cells and to predominantly cause the side reactions.[32–34] $^1O_2$ forms during discharge, rest, and from the onset of charge at rates that match the rates of parasitic chemistry occurring in cells. How $^1O_2$ forms is unclear but must be deeply rooted in the way (su)peroxides form or decompose.

Discharge commences with O_2 reduction to superoxide (MO_2). Whether it further reacts to the peroxide *via* a second electrochemical 1 e^- transfer

$$MO_2 + e^- + M^+ \rightarrow M_2O_2 \quad (2)$$

or disproportionation

$$2MO_2 \rightarrow M_2O_2 + O_2 \quad (3)$$

is governed by the relative thermodynamic stability of peroxide and superoxide with the respective cation as illustrated in Fig. 1a. Strong Lewis acids such as Li^+ or Na^+ favour the peroxide *versus* the superoxide, albeit only slightly for sodium.[4,14,28,31,35,36] K^+ and even weaker Lewis acids (*e.g.*, quaternary amines like tetrabutylammonium (TBA^+) and imidazoliums favour the superoxide.[10,37–39] The latter constitute often used ionic liquid electrolytes. Superoxide disproportionation (eqn (3)) is now accepted to be involved on discharge and charge of the peroxides.[1,2,9,30,36,37,40–43] For example, Li_2O_2 oxidation during charge commences with surface

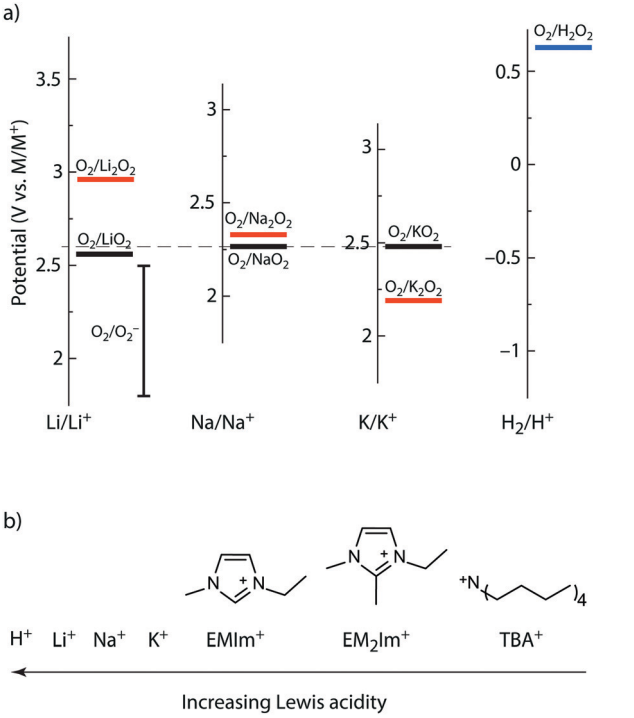

Fig. 1 Thermodynamics of alkali peroxides and superoxides and the Lewis acidity of the here used cations. (a) Standard potentials of the O_2/MO_2 and O_2/M_2O_2 redox couples on the M/M^+ scales with M = Li, Na, K as well as for the O_2/H_2O_2 couple. The scales are brought to a common scale based on their M/M^+ standard potentials. The dashed horizontal line indicates the O_2/KO_2 couple. The O_2/LiO_2 potential is adopted from ref. 45, but also values between 2.29 and 2.46 V *vs.* Li/Li^+ have been reported.[28,43] O_2/O_2^- denotes the potential range reported for O_2 reduction in TBA^+ electrolytes.[9,37,41,45,46] (b) Schematic Lewis acidity order of the used cations.

delithiation to form $Li_{2-x}O_2$ species or soluble superoxide, which release O_2 by disproportionation.[1,40,42,44] Large capacities require solution processes that favour the second electron transfer to/from peroxide to pass *via* disproportionation.[7–9,11,36,40,41] Pathways towards $^1O_2$ in this environment are unclear. Only better knowing the formation mechanism may allow finding strategies to inhibit $^1O_2$ formation, which is indispensable for progress towards fully reversible, high capacity metal–O_2 cells.

Here, we show that superoxide disproportionation in aprotic media releases significant fractions of $^1O_2$ and we derive mechanistic descriptors for $^1O_2$ *vs.* $^3O_2$ release backed by simulations. While the strong Lewis acids Li^+ and Na^+ stabilize peroxide *versus* superoxide and drive the overall reaction, the $^1O_2$ fraction is higher with Na^+, the weaker Lewis acid. Also present even weaker Lewis acids enhance the $^1O_2$ fraction massively. Larger $^1O_2$ fractions go along with smaller peroxide yield. The results explain a major degradation pathway, explain the growing parasitic chemistry in K–, Na–, and Li–O_2 cells based on the growing propensity for disproportionation, and show that counteracting $^1O_2$ formation requires finding reaction routes that avoid superoxide disproportionation. Given that large capacities and rates require solution processes that rely on disproportionation steps, the results establish a central dilemma for high capacity metal–O_2 cells.

Experimental

Materials

Salts contained either the bis(trifluoromethane)sulfonimide ($TFSI^-$) or ClO_4^- anion. These anions have similar donor numbers and exert therefore minor changes on the considered solution equilibria[47,48] and an analogous effect of TBA^+ addition as confirmed in Fig. S1 (ESI†). LiTFSI, $NaClO_4$, $KClO_4$, TBATFSI were dried under vacuum for 24 h at 80 °C. Dimethoxyethane (DME) and tetraethylene glycol dimethyl ether (TEGDME) were dried over lithium, distilled and further dried and stored over activated molecular sieves. The water content as measured by Karl–Fischer titration was below 5 ppm. 9,10-Dimethylanthracene (DMA) was recrystallized from ethanol. Lithium peroxide (Li_2O_2) was synthesized as described previously.[49] Its purity was confirmed by XRD, FTIR spectroscopy, and carbonate/carboxylate analysis.[50]

Electrochemical methods

Metal–O_2 cells with integrated pressure transducer were of the type PAT-Cell-Press from EL-Cell GmbH (Hamburg, Germany) with custom modified cathode plunger as described earlier.[51] Electrochemical tests were run on a potentiostat/galvanostat (SP-300 or MPG-2, Bio-Logic). Free standing carbon/PTFE electrodes were made from a slurry of Super P carbon/PTFE binder (9/1, w/w) using isopropanol. $Li_{1-x}FePO_4$/C black/PTFE (8/1/1, m/m) counter electrodes were prepared analogously. For the Li_2O_2/C/PTFE (1/8/1, m/m) electrodes, Li_2O_2 was first ground with Super P (1/9, m/m) for 1.5 h in a planetary ball mill (Pulverisette 7, Fritsch) at 200 rpm with ZrO_2 grinding balls under Ar. ATR-FTIR and XRD confirmed purity thereafter. A Super P/PTFE mixture (1/1, m/m) was made with isoproanol and dried under vacuum at 120 °C. Then, Li_2O_2/C and C/PTFE powders were mixed and pressed onto steel grids. Celgard separators and the electrodes were first washed with isoproanol and water (1/1, v/v) and subsequently with acetone. Electrodes and separators were dried under vacuum at 120 °C for 24 h. The counter electrode had three-fold the expected capacity of the working electrode. Typical working electrodes had a carbon mass loading of 1 mg and the cells were assembled with 100 μL electrolyte. Before discharge, cells were purged with high-purity O_2 (N5.0).

Spectroscopic methods

The mass spectrometry (MS) setup was built in-house and described previously.[33,50] The sample setup consisted of a glass vial with a volume of 7 mL equipped with a stirring bar. A PEEK plug with glued-in PEEK tubes and an exchangeable septum is sealed against the glass vial with a flat rubber seal. Reagents were added through a septum using a gas-tight syringe (Hamilton). All solutions were degassed with N_2 to remove dissolved CO_2 and O_2. The headspace was purged to the MS using 5 mL min^{-1} high purity Ar 6.0. To measure the rate of O_2 evolution during the disproportionation reaction, a high-precision pressure transducer (Omega, PAA35X) was connected to the closed vessel instead of the MS. Reagents were added with a gas-tight syringe through glued-in tubing.

High-performance liquid chromatography (HPLC) was used to determine the degree of the DMA-to-DMA-O_2 conversion as described earlier.[33] From chemical experiments, the filtered

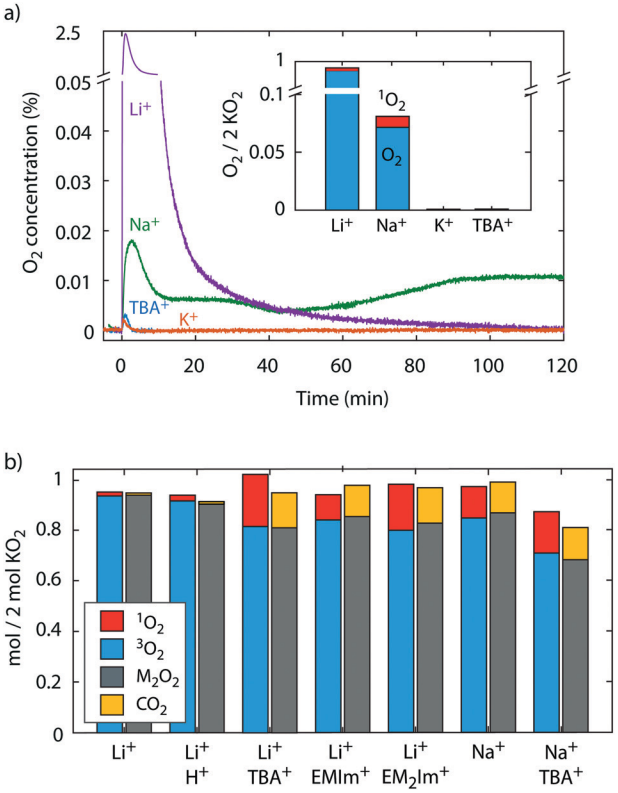

Fig. 2 $^1O_2$ from superoxide disproportionation in presence of various cations. (a) O_2 evolution *versus* time upon mixing KO_2 with TEGDME electrolytes containing 0.1 M of the indicated cations and 30 mM 9,10-dimethylanthracene (DMA). The inset shows the evolved $^3O_2$ (as measured by MS) and $^1O_2$ (as measured as DMA-O_2 by HPLC) after 2 h reaction time. (b) Obtained O_2, $^1O_2$, and Li_2O_2 (or Na_2O_2) upon reacting KO_2 in TEGDME that contained equimolar 18-crown-6, 30 mM DMA, 0.5 M Li^+ (or Na^+), and either no additive, 0.1 M TBA^+, $EMIm^+$, or EM_2Im^+, or F_3CCOOH. The scale means mol of O_2, $^1O_2$, Li_2O_2, or CO_2 per 2 mol of KO_2. *I.e.*, ideally 1 mol O_2 and 1 mol M_2O_2 would form according to $2KO_2 + 2M^+ \rightarrow M_2O_2 + O_2 + 2K^+$. Error bars are given in Fig. S4 (ESI†).

electrolyte was diluted with DME to ~1 mg_{DMA} mL^{-1}. From cells, the electrolyte was extracted from all cell components using 400 μL DME, sonicated for 10 min under exclusion of light and heat, centrifuged and the supernatant was transferred and DME removed under a N_2 stream at room temperature. The residue was dissolved in 500 μL DME and a volume of 2 μL was injected into the HPLC.

The amount of peroxide in a sample was measured by UV-vis spectroscopy of the Ti(IV)-peroxo complex in combination with mass spectrometry as described previously.[50] The acidic environment also evolves CO_2 from carbonates which was measured by MS. The samples in Fig. 2 and 3 from which Li_2O_2 and CO_2 yield were obtained were prepared separately to the ones for $^1O_2$ and $^3O_2$ yield since DMA is incompatible with the Ti(IV) peroxo complex. Measurements given in bar graphs are from typically three or more repetitions. Repeatability is illustrated in Fig. S4 (ESI†).

Computational methods

Energies were calculated for solvated species with a solvent dielectric constant of 7.28 (1,1,2-trichloroethane, a value close to short chain glymes, like DME) by density functional theory

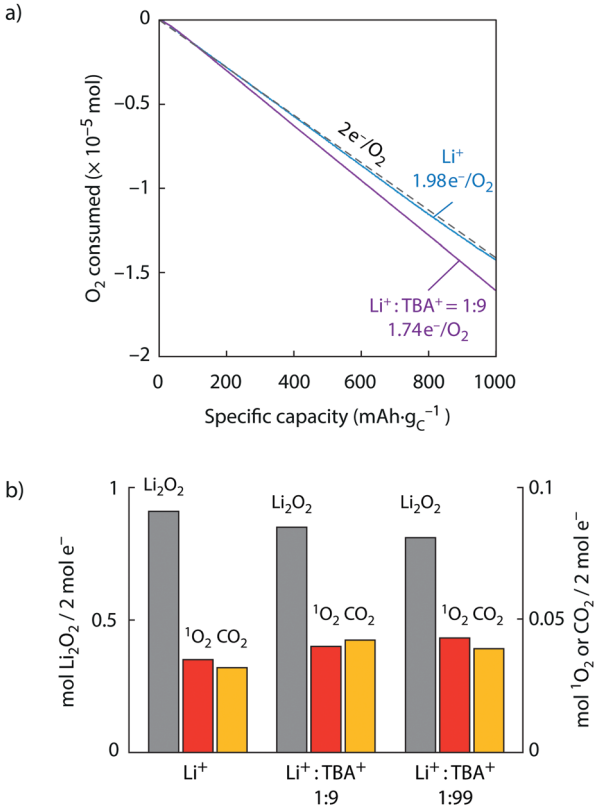

Fig. 3 Superoxide disproportionation and $^1O_2$ formation during Li–O_2 cell discharge. (a) O_2 consumption *vs.* capacity upon discharge of carbon black electrodes at a rate of 100 mA g_C^{-1} in O_2 saturated TEGDME electrolytes that contained 30 mM DMA and either 0.1 M Li^+ or a total of 1 M salt with a Li^+ : TBA^+ ratio of 1 : 9 or 1 : 99. The 1 : 99 ratio is given in Fig. S9 (ESI†) and voltage profiles in Fig. S10 (ESI†). (b) Obtained Li_2O_2, $^1O_2$, and Li_2CO_3 (expressed as CO_2) per 2 e^- passed in the cells shown in (a).

(DFT) calculations by adopting a computational approach validated previously and benchmarked on post-Hartree–Fock calculations.[16] The M06-2X functional and the 6-31++G(d,p) basis set (unrestricted)[52] was used and solvation effects incorporated using a self-consistent reaction field (SCRF) in continuum solvation model C-PCM.[53] The final computational accuracy for the reaction energies that do not involve the $^1O_2$ species is estimated to be 0.05 eV. The pure O_2 ($^1\Delta_g$) molecule computed at the unrestricted M062X level shows unsatisfactory geometry and frequencies, similarly to the B3LYP functional, due to the well-known spin-contamination problem.[54] This unavoidable computational limitation at DFT level leads to an underestimate of the $^3\Sigma_g^- \rightarrow {}^1\Delta_g$ energy difference and thus to a worse computational accuracy for all $^1O_2$ release reactions, estimated to 0.1–0.15 eV. All structures were relaxed to their energy ground state and vibrational stability checked for all the reported reagents, intermediates, and products. The Gibbs energy of each molecular/ionic species was calculated at 298 K by considering zero-point energies and thermal effects. All calculations were done using Gaussian16.[55] Superoxide dimers we checked for all symmetric and asymmetric cases for all four conformers suggested by Bryantsev *et al.*[56] and reported values are for the most stable ground state structures. The structures are shown in Fig. S2 and S3 (ESI†). The reaction energy for the precipitation to solid peroxides was calculated with thermochemical cycles starting from DFT calculations, the assessed thermodynamic properties of solid phases and for neutral atoms in the gas phase.[57] The thermodynamics of the $TBA^+O_2^-$ ion couple was calculated at the same level of theory by relaxing the solid ionic couple in the simulated solvent to a ground state minimum.[58]

Results and discussion

Probing singlet oxygen from superoxide disproportionation

We studied the disproportionation reaction

$$2O_2^- \rightarrow O_2^{2-} + x^3O_2 + (1-x)^1O_2 \quad (4)$$

in presence of the cations shown in Fig. 1b that cover a wide range of Lewis acidity. These are the alkali cations Li^+, Na^+, and K^+ as well as H^+ from common protic electrolyte impurities and organic cations that are common constituents in ionic liquid electrolytes. Next to tetrabutylammonium (TBA^+) we also used 3-ethyl-1-methyl-1*H*-imidazol-3-ium ($EMIm^+$) and 3-ethyl-1,2-dimethyl-1*H*-imidazol-3-ium (EM_2Im^+) as organic cations since they were used as cations in ionic liquid electrolytes and the Lewis acidity of $EMIm^+$ and EM_2Im^+ covers a range between TBA^+ and K^+.[19,37,39] As superoxide source we used both KO_2 as a chemical source and the electrochemical reactions during cycling of Li–O_2 cells.

As a bimolecular reaction, superoxide disproportionation passes *via* $M(O_2)_2M$ dimers (with M being any of the cation in Fig. 1b).[35,41,56] We hypothesize that the energetics of pathways to $^3O_2$ and $^1O_2$ will sensitively depend on the cations involved. Therefore, to learn about the reaction mechanism, we intentionally influence the intermediates by using, next to pure Li^+ or Na^+ electrolytes, also their mixtures with TBA^+ that itself would not drive disproportionation; the overall driving force to Li_2O_2 or Na_2O_2 remains unchanged while an asymmetric $M(O_2)_2TBA$ intermediate dimer can be expected to be destabilized due to weaker O_2^-–TBA^+ than O_2^-–M^+ interactions[9,37,45] and hence to change the energetics and relative yields of $^3O_2$ and $^1O_2$ evolution.

To probe for $^1O_2$, we used 9,10-dimethylanthracene (DMA) as a chemical trap that fulfils the requirements for the non-aqueous (electro)chemical environment: it selectively forms the endoperoxide (DMA-O_2) in contact with $^1O_2$. DMA and DMA-O_2 can be quantified by HPLC as detailed in the Methods, are electrochemically stable in the required potential range, and are stable towards superoxide and peroxide.[33,34]

Disproportionation of chemically produced superoxide

To probe for $^3O_2$ and $^1O_2$ yields from superoxide disproportionation, we first brought solid KO_2 in contact with Li^+, Na^+, K^+, and TBA^+ electrolytes based on tetraethyleneglycol dimethylether (TEGDME) that also contained DMA, Fig. 2a. TEGDME was used since it is a common solvent for metal–O_2 cells.[1,2,9,13] The reaction was done in a closed vessel with the head space continuously purged to a mass spectrometer (MS) for gas analysis and the DMA-to-DMA-O_2 conversion measured at the end of the experiment. When KO_2 was brought in contact with

the Li^+ electrolyte, the O_2 concentration rose sharply and ceased within 2 h, which indicates disproportionation as reported before.[9,23,41] Quantifying the total O_2 reveals that the KO_2 has nearly quantitatively reacted and has resulted in ~93% $^3O_2$ and ~2% $^1O_2$ of the total O_2 amount expected from eqn (4), *i.e.*, 1 mol O_2 per 2 mol KO_2. KO_2 in Na^+ electrolyte equally resulted in disproportionation as reported recently.[36] We found a continuous reaction, which does not come to completion within 2 h. The lower rate is in accord with the lower driving force (Fig. 1a) and the total O_2 after this time shows that ~8% of the KO_2 have reacted of which 12% resulted in $^1O_2$. KO_2 in contact with K^+ and TBA^+ electrolyte did not evolve an appreciable amount of O_2 as expected. These results show that superoxide disproportionation in presence of alkali cations yields significant fractions of $^1O_2$ with its fraction increasing as Lewis acidity of the cations decreases.

To avoid the complexities of reactions at a solid, we further investigated the disproportionation of KO_2 solvated by the crown ether 18-crown-6 (1,4,7,10,13,16-hexaoxacyclooctadecane). Additionally to $^3O_2$ and $^1O_2$, we also measured the Li_2O_2 or Na_2O_2 yield, respectively, after O_2 evolution ceased using established procedures with photometry of the $[Ti(O_2)OH]^+$ complex after adding acidic $TiOSO_4$ solution, which also evolves CO_2 from formed carbonate.[4,50] The CO_2 amount serves as a proxy for the amount of side products. We added either pure Li^+ electrolyte or combination of Li^+ with H^+, TBA^+, $EMIm^+$, or EM_2Im^+. We further added pure Na^+ or Na^+/TBA^+ electrolytes. The results are shown in Fig. 2b. The result with pure Li^+ resembles the one with solid KO_2 in Fig. 2a; the $^3O_2$ and Li_2O_2 yields were ~93% and the $^1O_2$ ~2%. With F_3CCOOH as H^+ source we found ~91% for $^3O_2$ and peroxide yield and 3% for $^1O_2$ yield and thus vanishingly more $^1O_2$ than without acid. This is in accord with reported minor $^1O_2$ yields from proton assisted superoxide disproportionation in Li-free media.[59,60]

Mixtures of Li^+ and the weakly Lewis acidic organic cations, however, increase $^1O_2$ very strongly; the $^3O_2$ and Li_2O_2 yields dropped to ~80–85% and the $^1O_2$ rose to ~10–20%. Carbonaceous side products as indicated by CO_2 evolution also rose similarly. Adding weak Lewis acids into the disproportionation reaction not only raised the $^1O_2$ yield massively, but concurrently boosted the reaction rates. We measured the $^3O_2$ evolution kinetics from superoxide disproportionation by means of the pressure rise in a closed reaction vessel (Fig. S5, ESI†). Values compared to the kinetics with Li^+ alone are 5-fold with $EMIm^+$ and TBA^+ and 8-fold with EM_2IM^+. The mechanistic implications of this finding are discussed later together with the theoretical results.

Given that organic cations provoke high $^1O_2$ amounts, we assessed their stability in the system. Tetraalkylammoniums have been shown previously to be stable with superoxide.[41] We probed whether imidazoliums would be reactive with superoxide or $^1O_2$ and whether they would quench the latter and thus reduce the DMA-O_2 yield, which then would underestimate the $^1O_2$ yield. When $EMIm^+$ and EM_2Im^+ were exposed to KO_2 in TEGDME for 1 h, ^{1}H-NMR spectra show a large number of new peaks (Fig. S6, ESI†), indicating decomposition in accord with previous reports.[61] Exposing imidazoliums for 1 h to $^1O_2$, generated photochemically as detailed in the Supplementary Methods (ESI†), left the ^{1}H-NMR spectra largely unchanged (Fig. S7, ESI†). We do, however, not exclude a certain reactivity. Imidazoliums in high concentrations show a noticeable ability to quench $^1O_2$ to $^3O_2$, which suggests that measured $^1O_2$ yields with imidazolium are likely underestimated (Fig. S8 and Supplementary Note 1, ESI†). Overall, enhanced $^1O_2$ formation and instability with superoxide both make imidazoliums unsuitable for metal–O_2 cells.

Turning to superoxide disproportionation in Na^+ and mixed Na^+/TBA^+ electrolytes, we find for pure Na^+ an analogous result to Fig. 2a: ~13% $^1O_2$, 85% $^3O_2$ and 87% Na_2O_2. For the mixed Na^+/TBA^+ electrolyte the $^3O_2$ and Na_2O_2 yields further dropped to around 70% and the $^1O_2$ rose to ~16%. Together with the results for Li^+/TBA^+ mixtures, the higher levels of $^1O_2$ with the less Lewis acidic Na^+ suggest that weaker Lewis acidic cations favour $^1O_2$ evolving pathways. Another common result for all conditions in Fig. 2b is that the amounts of $^3O_2$ and alkali peroxide closely match each other and that a larger fraction of missing peroxide is related to a larger amount of $^1O_2$ formed.

Disproportionation during Li–O_2 cell cycling

To probe whether the above observed disproportionation phenomena that yield $^1O_2$ also explain $^1O_2$ formation in cells, we performed analogous electrochemical experiments in Li–O_2 cells. Li–O_2 was chosen since disproportionation is most significantly driven by thermodynamics (Fig. 1a). We focus on TBA^+ as the weak Lewis acid since it avoids the further complications of imidazolium instability with O_2^-. Considering first discharge, we constructed cells as detailed in the Experimental section with carbon black cathodes and TEGDME electrolytes containing 30 mM DMA and either only 0.1 M Li^+ or a total of 1 M salt with a Li^+:TBA^+ ratio of 1:9 or 1:99. The cells were discharged at constant current and the O_2 consumption followed using a pressure transducer as shown in Fig. 3a and Fig. S9 (ESI†). At the end of discharge, electrolyte and cathodes were extracted and analysed for the amount of $^1O_2$, Li_2O_2, and carbonate. The results are shown in Fig. 3b with all values expressed as mol per 2 mol e^- passed. Hence, ideally 2 mol e^- would give 1 mol Li_2O_2 according to eqn (1).

Discharge in pure Li^+ electrolyte resulted in a ratio of 1.98 e^-/O_2, close to the ideal ratio of 2, and a Li_2O_2 yield of 94%, which both is in accord with previous reports for similar cells.[11,15,20–22,33,50] The $^1O_2$ yield was ~3% and hence similar to that found in Fig. 2 for O_2^- disproportionation in Li^+ electrolyte. With mixed Li^+/TBA^+ electrolytes with a Li^+:TBA^+ ratio of 1:9 (1:99), the e^-/O_2 ratio and Li_2O_2 yield dropped to 1.74 (1.70) e^-/O_2 and 85% (81%), respectively. Concurrently, the amount of $^1O_2$ and carbonate increased as the Li_2O_2 yield decreased. Increasing $^1O_2$ yield together with decreasing Li_2O_2 yield as the electrolyte is changed from Li^+ to Li^+/TBA^+ mix mirrors the results in Fig. 2 for the chemical experiments. Considering further the e^-/O_2 ratios, the ideal value of 2 results from the sinks for the initially formed O_2^-: a second 1 e^- reduction to peroxide or disproportionation to $^3O_2$, which both give an overall 2 e^-/O_2 process. e^-/O_2 ratios lower than 2 imply more efficient sinks to exist for the 1 e^- product O_2^- than a

second reduction or disproportionation to $^3O_2$. Given the known stability of TBA^+ with O_2^-,[36,41] their reaction can be excluded as the sink to cause the decrease to 1.74 (1.70) e^-/O_2. Instead, the lower ratio is in accord with TBA^+ enhancing the $^1O_2$ fraction from O_2^- disproportionation. Discharge with imidazoliums instead of TBA^+ further corroborates their unsuitability as seen in even lower e^-/O_2 ratios of 1.42 and 1.2 for EM_2Im^+ and $EMIm^+$, respectively (Supplementary Note 2 and Fig. S11, ESI†). The results on discharge are in accord with the chemical experiments shown in Fig. 2, which have shown that O_2^- disproportionation partly releases $^1O_2$ and that the $^1O_2$ fraction increases with the presence of TBA^+. Overall, the results show that O_2^- disproportionation is the source of $^1O_2$ on discharge, which further implies that discharge in the investigated TEGDME electrolyte passes at least significantly *via* disproportionation next to a possible second 1 e^- reduction of the LiO_2 intermediate *via* eqn (2).

Turning to cell charge, we probed whether TBA^+ analogously reveals $^1O_2$ formation by O_2^- disproportionation. $Li_{2-x}O_2$ or soluble superoxide species were reported as intermediates on charge that disproportionate to form Li_2O_2 and O_2.[1,40,42,43] This reaction may hence equally be the source of $^1O_2$ and sensitive to cations. We constructed Li_2O_2-packed working electrodes as detailed in the Experimental section. Li_2O_2 was ball milled with carbon black to ensure intimate contact between the two and the resulting powder was used to form composite electrodes using PTFE binder. We charged them in electrolytes that contained either only Li^+ or a Li^+/TBA^+ mix and measured the amount of $^3O_2$ and $^1O_2$ by means of the pressure in the cell head space and DMA conversion, Fig. 4. The charge voltage was limited to 3.95 V since this voltage was reported to be the upper limit for quasi-equilibrium decomposition in TEGDME.[40] Pressure evolution with pure Li^+ electrolyte (Fig. 4a) shows similarly to previous reports[11,20,21,40] an elevated value of 2.40 e^-/O_2 and thus ~83% of the expected O_2 evolved based on charge passed. $^1O_2$ formation shows that the $^3O_2$ loss is connected with $^1O_2$ formation. When Li_2O_2 was charged in Li^+/TBA^+ electrolyte (Fig. 4b), the e^-/O_2 ratio rose to 2.95 and hence only ~68% of the expected $^3O_2$ evolved. Roughly doubled missing $^3O_2$ evolution goes along with the $^1O_2$ amount being more than doubled. To exclude the suggested $^1O_2$ evolution from a direct 2 e^- oxidation of Li_2O_2 above 3.5 V,[32] we also restricted the charging voltage to 3.45 V, which shows similar results as with charge limited to 3.95 V (Supplementary Note 3, ESI†). Analogously to the experiments on discharge (Fig. 3), presence of TBA^+ increased the fraction of $^1O_2$ from O_2^- disproportionation with concurrently dropping $^3O_2$ fraction. Proportional correlation between missing $^3O_2$ evolution and $^1O_2$ yield suggest in either case superoxide disproportionation to be a major O_2 evolution and $^1O_2$ generation pathway.

Taken together, the results from the chemical and electrochemical experiments show that superoxide disproportionation, driven by the higher stability of the peroxide with strong Lewis acids, generates in part $^1O_2$. Simultaneous presence of weakly Lewis acidic organic cations increases the $^1O_2$ yield markedly in the chemical and electrochemical experiments. These results (a) corroborate that superoxide disproportionation is a main pathway for the second electron transfer from superoxide to peroxide during discharge and O_2 evolution during charge and (b) show that superoxide disproportionation is the $^1O_2$ source during cell cycling.

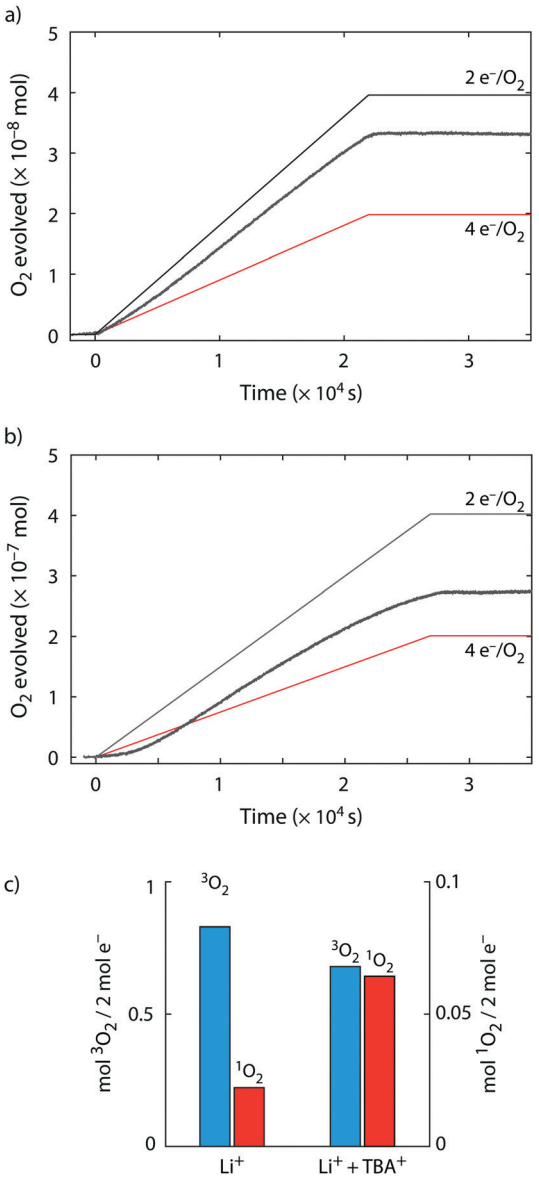

Fig. 4 Superoxide disproportionation and $^1O_2$ formation during Li–O_2 cell charge. (a and b) O_2 evolution *vs.* time upon charge of carbon black/Li_2O_2/PTFE (9/1/1, m/m) composite electrodes in TEGDME electrolyte containing 30 mM DMA and 0.1 M Li^+ (a) or 0.1 M Li^+ and 0.9 M TBA^+ (b). Electrodes were charged at a rate of 10 mA g_C^{-1} until 3.95 V and then kept at open circuit until the pressure was stable. (c) $^3O_2$ and $^1O_2$ obtained per 2 e^- passed for the cells shown in (a) and (b).

A direct consequence of this finding is that the extent to which $^1O_2$ can form on discharge and charge is governed by the extent to which disproportionation is responsible for the second electron transfer. The latter has been subject to many important studies recently and current understanding is that dominance of one or the other is governed by the LiO_2 solvation *vs.* surface adsorption.[2,62] Except for very poorly LiO_2 solvating

electrolytes such as MeCN, disproportionation appears to dominate even in only slightly more solvating glymes and certainly in any solvent with higher donor number, which is further enhanced by Li salt anions that dissociate weakly.[6,63] Partition between second reduction/disproportionation has been, for example, investigated in glyme and DMSO by Shao-Horn who found at least significant disproportionation in glyme at low overpotentials.[64] Peng calculated potentials where O_2^-* could be directly reduced to Li_2O_2* in DMSO and found disproportionation to dominate above 2 V *vs.* Li/Li^+ on Au(111). Considering the latter, catalysts could potentially favour a second electron transfer already at higher voltages. We are, however, not aware of any study showing this possibility on discharge, but recent work by Lu suggests that catalysts could favour direct oxidation on charge.[40,65,66] Another potential way could be redox mediators as suggested for quinones on discharge.[7,8] However, proof that this fully suppresses superoxide disproportionation is still missing.

Energetics of singlet oxygen generation

To better understand the energetics of disproportionation and particularly why weak Lewis acids boost $^1O_2$ formation, we performed density functional theory (DFT) calculations for pathways leading to $^3O_2$ and $^1O_2$. We considered LiO_2 and NaO_2 disproportionation as well as the asymmetric pairings of LiO_2 and NaO_2 with HO_2 and $TBAO_2$. Energies were calculated for solvated species using the continuous C-PCM solvation model with a mean dielectric constant of ε = 7.28 (resembling glyme) and using the hybrid GGA DFT M06-2X functional and the most favourable pathways are shown in Fig. 5. All energies are relative to the free superoxide monomers ($2LiO_2$ or $2NaO_2$) to help understanding how cations other than Li^+ or Na^+ change the energetics relative to pure Li^+ or Na^+ electrolytes due to ion association/dissociation equilibria. A reaction energy $\Delta_r G^\circ_{298K}$ beyond 1 eV implies an at least as high activation barrier and hence slow kinetics at room temperature.[18] Starting from the doublet superoxide monomers, reactions may follow singlet or triplet pathways through the formation of a superoxide dimer $M(O_2)_2M'$ (M being Li^+ or Na^+, and M′ being M, H^+ or TBA^+). The dimers release singlet or triplet O_2 and singlet MO_2M' peroxide that may further ion exchange to M_2O_2 and precipitate as solid $M_2O_{2(s)}$.

We consider first the symmetric LiO_2 and NaO_2 cases (Fig. 5a and b, red traces). For LiO_2, the triplet $^3Li(O_2)_2Li$ dimer is slightly stabilized compared to two monomers and releases Li_2O_2 + $^3O_2$ weakly endergonic, followed by strongly stabilizing Li_2O_2 precipitation to solid $Li_2O_{2(s)}$, which is the main overall driving force (Fig. 5a). Our results are in accord with previous works that analysed the route from LiO_2 to $^3O_2$ in the gas[35,56] and solution phase[41] and which are summarized in Fig. S13 (ESI†) for comparison. The path that we find for $^1O_2$ release appears possible but slower with a thermodynamic barrier of ~1 eV to the singlet $^1Li(O_2)_2Li$ dimer followed by downhill $^1O_2$ release and $Li_2O_{2(s)}$ precipitation. The symmetric NaO_2 case (Fig. 5b) is in either case uphill to the dimers but with their order being reversed (relative energies of singlet/triplet $M(O_2)_2M$ dimers are analysed in detail in Supplementary Note 4, ESI†);

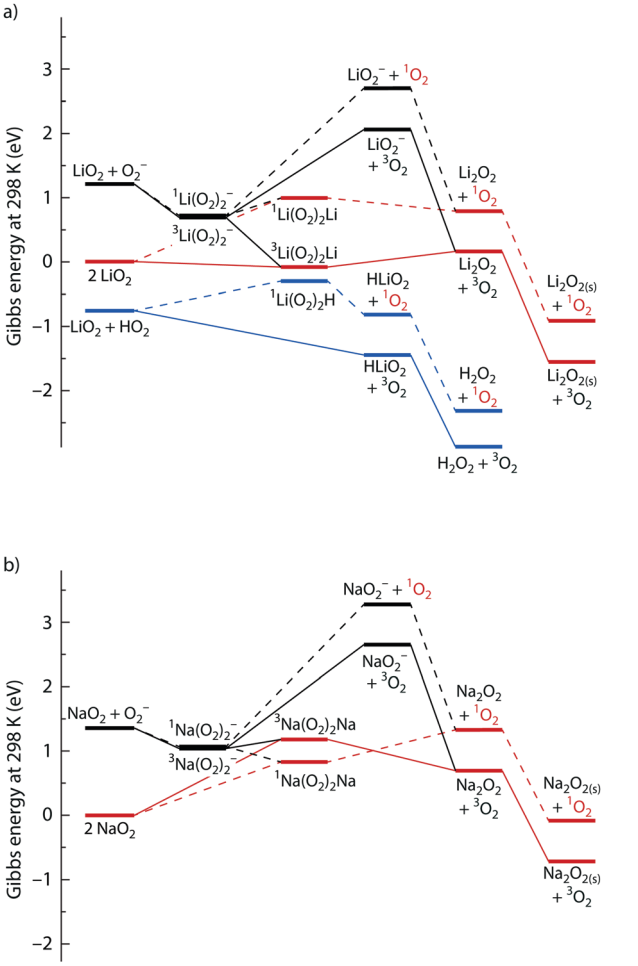

Fig. 5 Reaction free energy profiles for superoxide disproportionation. (a) LiO_2 disproportionation with itself, O_2^- or HO_2 to Li_2O_2 and molecular oxygen. (b) NaO_2 disproportionation with itself or O_2^- to Na_2O_2 and molecular oxygen. Pathways to release $^3O_2$ and $^1O_2$ are indicated by full and dashed lines, respectively. All species are computed in the solvated state except for the final solid peroxide. The computational method is M06-2X6-31**G++C-PMD (ε = 7.28). Numerical values are given in Tables S2–S4 (ESI†). Further asymmetric alkali superoxide pairings are considered in Supplementary Note 5 (ESI†).

the singlet $^1Na(O_2)_2Na$ dimer forms with an energy increase of 0.83 eV less endergonic than the triplet $^3Na(O_2)_2Na$ with ~1.2 eV barrier. However, ongoing $^1O_2$ release is further endergonic by 0.5 eV while $^3O_2$ release is exergonic by −0.5 eV. The single step thermodynamic barrier towards $^1O_2$ release from NaO_2 is hence ~0.1 eV higher than the barrier towards $^3O_2$. The following precipitation of solid $Na_2O_{2(s)}$ makes both singlet and triplet path overall exergonic, but less than for LiO_2 disproportionation. Together, the relative single step barriers and overall driving forces rationalize our experimental findings: LiO_2 disproportionates fast and the strongly differing barriers between singlet and triplet path cause relatively small $^1O_2$ fractions. NaO_2 disproportionates slowly and the more similar barriers cause larger $^1O_2$ fractions.

Turning to proton mediated O_2^- disproportionation, our thermodynamic calculations for the asymmetric LiO_2 + HO_2 pairing suggest much easier $^3O_2$ than $^1O_2$ formation (Fig. 5a, blue traces).

$^3O_2$ and the mixed $HLiO_2$ peroxide form in an exergonic single step reaction ($\Delta_r G^\circ_{298K} = -0.7$ eV) without a stable intermediate dimer. In contrast, the singlet path faces a barrier of 0.46 eV to the singlet $^1Li(O_2)_2H$ dimer, which releases $HLiO_2$ and $^1O_2$ in a by −0.52 eV exergonic step. Analogous results were obtained for the $NaO_2 + HO_2$ pairing (Fig. S14, ESI†). The singlet path is in either case much more demanding and will result in minor $^1O_2$ yields. This is in accord with our experimental finding in Fig. 2, which shows insignificant additional $^1O_2$ with protons compared to pure Li^+ electrolyte. It is also in accord with reported negligible $^1O_2$ yields from proton mediated O_2^- disproportionation in Li^+ and Na^+ free media.[59,60] We conclude from the calculations, in accord with the experiments, that proton sources cause minor additional $^1O_2$ compared to disproportionation in Li^+ electrolyte.

Turning to the case of the asymmetric pairing of superoxide with Li^+ and the weakly Lewis acidic TBA^+, our initial hypothesis was that weaker O_2^-–TBA^+ than O_2^-–M^+ interactions[9,37,45] would destabilize intermediates, reduce barriers, and hence make $^1O_2$ more favourable. In support of that, the experiments have shown higher kinetics and $^1O_2$ yields with TBA^+ (Fig. 2–4 and Fig. S5, ESI†) and the calculations in Fig. 5 confirm the suggested reasons. Considering the weak association of the $TBA^+O_2^-$ ion pair even in low dielectric constant solvents like DME ($\Delta_{diss}G^\circ_{298K} = 0.44$ eV), $TBAO_2$ may be approximated by the free solvated O_2^- anion. Solvent dependent O_2/LiO_2 and $O_2/TBAO_2$ standard potentials have been measured and computed by Shao-Horn *et al.*[45] and found to differ by 1.24 V in DME, which agrees well with our estimate of 1.21 eV for the dissociation energy of LiO_2 to free O_2^- anions (Fig. 5a, black traces). Note that O_2^- does not have to form *via* dissociation of LiO_2, but may form as a transient species upon O_2^- generation. Ongoing triplet and singlet paths initially form $^3Li(O_2)_2^-$ and $^1Li(O_2)_2^-$ dimers that are stabilized *versus* $LiO_2 + O_2^-$ by −0.52 eV and −0.49 eV, respectively. Ongoing pathways to the charged LiO_2^- peroxide species plus $^1O_2$ or $^3O_2$ would face prohibitively high barriers because of the large dissociation energy of $Li_2O_2 \rightarrow LiO_2^- + Li^+$. Instead, our calculations reveal other facile pathways: the $Li(O_2)_2^-$ dimers can easily exchange TBA^+ for Li^+ and hence feed into the symmetric $Li(O_2)_2Li$ pathways discussed above and shown in the red traces in Fig. 5a. Crucially, the presence of TBA^+ decreases the barrier towards $^1O_2$, the endergonicity of the most unfavourable step to the $^1Li(O_2)_2Li$ dimer, from ∼1 eV to a mere 0.27 eV. Analogously, the asymmetric $NaO_2 + O_2^-$ pairing passes *via* $Na(O_2)_2^-$ and $Na(O_2)_2Na$ dimers and the barrier towards $^1O_2$ decreases from 1.2 eV to 0.4 eV. Overall, the weak Lewis acid TBA^+ opens paths to bypass the most unfavourable reaction steps und hence strongly facilitates $^1O_2$ evolution.

Consequences for metal–O_2 batteries

Recognizing that $^1O_2$ formation is deeply rooted in the way current metal–O_2 cells operate has serious consequences on aspects to avoid and on directions that should be gone. First, caution must be exercised with weak Lewis acids as electrolytes or additives. This is supported by the selected quaternary ammonium and imidazolium cations, which are prototypical motifs for the cations used so far in ionic liquid electrolytes for metal–O_2 cells. Imidazoliums readily decompose with superoxide. Significantly, we could show that the organic cation's weak Lewis acidity rather than its chemical nature massively boosts $^1O_2$ formation. Given that ionic liquid cations suitable for electrolytes are most typically weak Lewis acids, the effect can likely be generalized. Favoured $^1O_2$ formation explains why quantitative studies of metal–O_2 chemistry with a broad variety of ionic liquids have shown worse parasitic chemistry on discharge and charge than molecular electrolytes.[19,20,24]

Second, protic additives drive $^1O_2$ formation insignificantly but may drive parasitic chemistry in other ways. This is in accord with reports that found increased side reactions when water or other Brønsted acids were added.[11,29,67] The previous suggestion that proton sources could cause $^1O_2$ in Na–O_2 cells[34] can now be revised to NaO_2 disproportionation being the $^1O_2$ source. Protons may be a remaining source of instability in K–O_2 cells despite thermodynamic stability of KO_2 in K^+ electrolytes.[5,10,26,38] Meticulously excluding impurities has hence allowed for impressive cyclability of K–O_2 batteries.[5]

Finally, the most prominent consequence is that situations bound for superoxide disproportionation must be avoided. Cells based on metastable LiO_2 or NaO_2 as target products likely lack the practically required tolerance to slow discharge and rest periods; the superoxides gradually convert to peroxide and side products.[3,14,25,27,30,34,35] Peroxide products are preferred as they are much higher in energy density and the thermodynamically stable products.[28,31,68] Cycling them highly reversible requires finding routes to form and decompose them without superoxide disproportionation steps. Potential ways to do so are catalysts[40,65,66] or redox mediators.[7,8]

Conclusions

In conclusion, we describe the mechanism for $^1O_2$ formation and hence a main driver parasitic chemistry across alkali metal–O_2 cells. We show that superoxide disproportionation forms the $^1O_2$, and we clarify the reaction mechanism and governing factors in detail. The mechanism explains the growing parasitic chemistry in K–, Na–, and Li–O_2 cells as well as between superoxide and peroxide products based on the growing propensity for disproportionation. The strong Lewis acids H^+, Li^+ and Na^+ stabilize peroxide *versus* superoxide and hence drive disproportionation. $^1O_2$ yields grow in this order with H^+ causing insignificant $^1O_2$ and strongly growing $^1O_2$ fractions with Li^+ and Na^+. Importantly, weak Lewis acids such as TBA^+ alone do not drive disproportionation, but, when combined with strong Lewis acids, strongly reduce the reaction barriers towards $^1O_2$ and cause substantially larger fractions of $^1O_2$. This calls for caution with ionic liquid electrolytes that comprise such weak Lewis acidic cations. The results explain major degradation routes of metal–O_2 cells. Given that achieving high capacities and rates requires solution routes on discharge and charge, which in turn favour disproportionation reactions, the results establish the central dilemma that disproportionation is both important for

high capacity/high rate and responsible for degradation. Future work should hence focus on finding routes for peroxide discharge and charge that avoid superoxide disproportionation.

Authors contributions

E. M., Y. K. P., A. S., C. L., N. M., S. A. F. developed the methods and/or did the experiments. R. S., F. F. S., S. B. did calculations. C. P., C. S., O. F., S. B., S. A. F. discussed the results. S. A. F. and S. B. conceived the work and wrote the paper.

Conflicts of interest

There are no conflicts to declare.

Acknowledgements

S. A. F. is indebted to the European Research Council (ERC) under the European Union's Horizon 2020 research and innovation program (grant agreement no. 636069) and the Austrian Federal Ministry of Science, Research and Economy and the Austrian Research Promotion Agency (grant no. 845364). We thank EL-Cell GmbH (Hamburg, Germany) for the test cells. Likewise, we thank M. Winkler of Acib GmbH and G. Strohmeier for HPLC measurements, S. Borisov, W. Yin, and A. Grimaud for discussions, and R. Saf for help with the MS.

Notes and references

1 Y.-C. Lu, B. M. Gallant, D. G. Kwabi, J. R. Harding, R. R. Mitchell, M. S. Whittingham and Y. Shao-Horn, *Energy Environ. Sci.*, 2013, **6**, 750–768.
2 D. Aurbach, B. D. McCloskey, L. F. Nazar and P. G. Bruce, *Nat. Energy*, 2016, **1**, 16128.
3 T. Liu, G. Kim, M. T. L. Casford and C. P. Grey, *J. Phys. Chem. Lett.*, 2016, **7**, 4841–4846.
4 P. Hartmann, C. L. Bender, M. Vračar, A. K. Dürr, A. Garsuch, J. Janek and P. Adelhelm, *Nat. Mater.*, 2012, **12**, 228–232.
5 G. Cong, W. Wang, N.-C. Lai, Z. Liang and Y.-C. Lu, *Nat. Mater.*, 2019, **18**, 390–396.
6 C. M. Burke, V. Pande, A. Khetan, V. Viswanathan and B. D. McCloskey, *Proc. Natl. Acad. Sci. U. S. A.*, 2015, **112**, 9293–9298.
7 X. Gao, Y. Chen, L. Johnson and P. G. Bruce, *Nat. Mater.*, 2016, **15**, 882–888.
8 T. Liu, J. T. Frith, G. Kim, R. N. Kerber, N. Dubouis, Y. Shao, Z. Liu, P. C. M. M. Magusin, M. T. L. Casford, N. Garcia-Araez and C. P. Grey, *J. Am. Chem. Soc.*, 2018, **140**, 1428–1437.
9 L. Johnson, C. Li, Z. Liu, Y. Chen, S. A. Freunberger, J.-M. Tarascon, P. C. Ashok, B. B. Praveen, K. Dholakia and P. G. Bruce, *Nat. Chem.*, 2014, **6**, 1091–1099.
10 W. Wang, N.-C. Lai, Z. Liang, Y. Wang and Y.-C. Lu, *Angew. Chem., Int. Ed.*, 2018, **57**, 5042–5046.
11 N. B. Aetukuri, B. D. McCloskey, J. M. García, L. E. Krupp, V. Viswanathan and A. C. Luntz, *Nat. Chem.*, 2014, **7**, 50–56.
12 C. Xia, R. Black, R. Fernandes, B. Adams and L. F. Nazar, *Nat. Chem.*, 2015, **7**, 496–501.
13 L. Lutz, W. Yin, A. Grimaud, D. Alves Dalla Corte, M. Tang, L. Johnson, E. Azaceta, V. Sarou-Kanian, A. J. Naylor, S. Hamad, J. A. Anta, E. Salager, R. Tena-Zaera, P. G. Bruce and J.-M. Tarascon, *J. Phys. Chem. C*, 2016, **120**, 20068–20076.
14 I. Landa-Medrano, R. Pinedo, X. Bi, I. Ruiz de Larramendi, L. Lezama, J. Janek, K. Amine, J. Lu and T. Rojo, *ACS Appl. Mater. Interfaces*, 2016, **8**, 20120–20127.
15 B. D. Adams, R. Black, Z. Williams, R. Fernandes, M. Cuisinier, E. J. Berg, P. Novak, G. K. Murphy and L. F. Nazar, *Adv. Energy Mater.*, 2015, **5**, 1400867.
16 M. Carboni, A. G. Marrani, R. Spezia and S. Brutti, *Chem. – Eur. J.*, 2016, **22**, 17188–17203.
17 R. Black, A. Shyamsunder, P. Adeli, D. Kundu, G. K. Murphy and L. F. Nazar, *ChemSusChem*, 2016, **9**, 1795–1803.
18 V. S. Bryantsev, V. Giordani, W. Walker, M. Blanco, S. Zecevic, K. Sasaki, J. Uddin, D. Addison and G. V. Chase, *J. Phys. Chem. A*, 2011, **115**, 12399–12409.
19 S. Das, J. Højberg, K. B. Knudsen, R. Younesi, P. Johansson, P. Norby and T. Vegge, *J. Phys. Chem. C*, 2015, **119**, 18084–18090.
20 B. D. McCloskey, D. S. Bethune, R. M. Shelby, T. Mori, R. Scheffler, A. Speidel, M. Sherwood and A. C. Luntz, *J. Phys. Chem. Lett.*, 2012, **3**, 3043–3047.
21 B. D. McCloskey, J. M. Garcia and A. C. Luntz, *J. Phys. Chem. Lett.*, 2014, **5**, 1230–1235.
22 B. D. McCloskey, A. Valery, A. C. Luntz, S. R. Gowda, G. M. Wallraff, J. M. Garcia, T. Mori and L. E. Krupp, *J. Phys. Chem. Lett.*, 2013, **4**, 2989–2993.
23 R. Black, S. H. Oh, J.-H. Lee, T. Yim, B. Adams and L. F. Nazar, *J. Am. Chem. Soc.*, 2012, **134**, 2902–2905.
24 M. Piana, J. Wandt, S. Meini, I. Buchberger, N. Tsiouvaras and H. A. Gasteiger, *J. Electrochem. Soc.*, 2014, **161**, A1992–A2001.
25 J. Kim, H. Park, B. Lee, W. M. Seong, H.-D. Lim, Y. Bae, H. Kim, W. K. Kim, K. H. Ryu and K. Kang, *Nat. Commun.*, 2016, **7**, 10670.
26 N. Xiao, R. T. Rooney, A. A. Gewirth and Y. Wu, *Angew. Chem., Int. Ed.*, 2018, **57**, 1227–1231.
27 S. Y. Sayed, K. P. C. Yao, D. G. Kwabi, T. P. Batcho, C. V. Amanchukwu, S. Feng, C. V. Thompson and Y. Shao-Horn, *Chem. Commun.*, 2016, **52**, 9691–9694.
28 C. L. Bender, P. Hartmann, M. Vračar, P. Adelhelm and J. Janek, *Adv. Energy Mater.*, 2014, **4**, 1–10.
29 K. U. Schwenke, M. Metzger, T. Restle, M. Piana and H. A. Gasteiger, *J. Electrochem. Soc.*, 2015, **162**, A573–A584.
30 D. Zhai, H.-H. Wang, J. Yang, K. C. Lau, K. Li, L. A. Curtiss and K. Amine, *J. Am. Chem. Soc.*, 2013, **135**, 15364–15372.
31 C. L. Bender, D. Schröder, R. Pinedo, P. Adelhelm and J. Janek, *Angew. Chem., Int. Ed.*, 2016, **55**, 4640–4649.
32 J. Wandt, P. Jakes, J. Granwehr, H. A. Gasteiger and R.-A. Eichel, *Angew. Chem., Int. Ed.*, 2016, **55**, 6892–6895.
33 N. Mahne, B. Schafzahl, C. Leypold, M. Leypold, S. Grumm, A. Leitgeb, G. A. Strohmeier, M. Wilkening, O. Fontaine, D. Kramer, C. Slugovc, S. M. Borisov and S. A. Freunberger, *Nat. Energy*, 2017, **2**, 17036.

34 L. Schafzahl, N. Mahne, B. Schafzahl, M. Wilkening, C. Slugovc, S. M. Borisov and S. A. Freunberger, *Angew. Chem., Int. Ed.*, 2017, **56**, 15728–15732.
35 U. Das, K. C. Lau, P. C. Redfern and L. A. Curtiss, *J. Phys. Chem. Lett.*, 2014, **5**, 813–819.
36 C. Sheng, F. Yu, Y. Wu, Z. Peng and Y. Chen, *Angew. Chem., Int. Ed.*, 2018, **57**, 9906–9910.
37 C. J. Allen, J. Hwang, R. Kautz, S. Mukerjee, E. J. Plichta, M. A. Hendrickson and K. M. Abraham, *J. Phys. Chem. C*, 2012, **116**, 20755–20764.
38 Y. Chen, Z. P. Jovanov, X. Gao, J. Liu, C. Holc, L. R. Johnson and P. G. Bruce, *J. Electroanal. Chem.*, 2018, **819**, 542–546.
39 C. V. Amanchukwu, H.-H. Chang, M. Gauthier, S. Feng, T. P. Batcho and P. T. Hammond, *Chem. Mater.*, 2016, **28**, 7167–7177.
40 Y. Wang, N.-C. Lai, Y.-R. Lu, Y. Zhou, C.-L. Dong and Y.-C. Lu, *Joule*, 2018, **2**, 2364–2380.
41 Y. Zhang, X. Zhang, J. Wang, W. C. McKee, Y. Xu and Z. Peng, *J. Phys. Chem. C*, 2016, **120**, 3690–3698.
42 S. Ganapathy, B. D. Adams, G. Stenou, M. S. Anastasaki, K. Goubitz, X.-F. Miao, L. F. Nazar and M. Wagemaker, *J. Am. Chem. Soc.*, 2014, **136**, 16335–16344.
43 S. Kang, Y. Mo, S. P. Ong and G. Ceder, *Chem. Mater.*, 2013, **25**, 3328–3336.
44 Y.-C. Lu and Y. Shao-Horn, *J. Phys. Chem. Lett.*, 2012, **4**, 93–99.
45 D. G. Kwabi, V. S. Bryantsev, T. P. Batcho, D. M. Itkis, C. V. Thompson and Y. Shao-Horn, *Angew. Chem., Int. Ed.*, 2016, **55**, 3129–3134.
46 Z. Peng, S. A. Freunberger, L. J. Hardwick, Y. Chen, V. Giordani, F. Bardé, P. Novák, D. Graham, J.-M. Tarascon and P. G. Bruce, *Angew. Chem., Int. Ed.*, 2011, **50**, 6351–6355.
47 M. Schmeisser, P. Illner, R. Puchta, A. Zahl and R. van Eldik, *Chem. – Eur. J.*, 2012, **18**, 10969–10982.
48 W. Linert, A. Camard, M. Armand and C. Michot, *Coord. Chem. Rev.*, 2002, **226**, 137–141.
49 M. M. Ottakam Thotiyl, S. A. Freunberger, Z. Peng and P. G. Bruce, *J. Am. Chem. Soc.*, 2013, **135**, 494–500.
50 B. Schafzahl, E. Mourad, L. Schafzahl, Y. K. Petit, A. R. Raju, M. O. Thotiyl, M. Wilkening, C. Slugovc and S. A. Freunberger, *ACS Energy Lett.*, 2017, **3**, 170–176.
51 Y. K. Petit, C. Leypold, N. Mahne, E. Mourad, L. Schafzahl, C. Slugovc, S. M. Borisov and S. A. Freunberger, *Angew. Chem., Int. Ed.*, 2019, **58**, 6535–6539.
52 Y. Zhao and D. G. Truhlar, *Theor. Chem. Acc.*, 2008, **120**, 215–241.
53 M. Cossi, N. Rega, G. Scalmani and V. Barone, *J. Comput. Chem.*, 2003, **24**, 669–681.
54 M. González, R. Valero, J. M. Anglada and R. Sayós, *J. Chem. Phys.*, 2001, **115**, 7015–7031.
55 M. J. Frisch, G. W. Trucks, H. B. Schlegel, G. E. Scuseria, M. A. Robb, J. R. Cheeseman, G. Scalmani, V. Barone, G. A. Petersson, H. Nakatsuji, X. Li, M. Caricato, A. V. Marenich, J. Bloino, B. G. Janesko, R. Gomperts, B. Mennucci, H. P. Hratchian, J. V. Ortiz, A. F. Izmaylov, J. L. Sonnenberg, Williams, F. Ding, F. Lipparini, F. Egidi, J. Goings, B. Peng, A. Petrone, T. Henderson, D. Ranasinghe, V. G. Zakrzewski, J. Gao, N. Rega, G. Zheng, W. Liang, M. Hada, M. Ehara, K. Toyota, R. Fukuda, J. Hasegawa, M. Ishida, T. Nakajima, Y. Honda, O. Kitao, H. Nakai, T. Vreven, K. Throssell, J. A. Montgomery, Jr., J. E. Peralta, F. Ogliaro, M. J. Bearpark, J. J. Heyd, E. N. Brothers, K. N. Kudin, V. N. Staroverov, T. A. Keith, R. Kobayashi, J. Normand, K. Raghavachari, A. P. Rendell, J. C. Burant, S. S. Iyengar, J. Tomasi, M. Cossi, J. M. Millam, M. Klene, C. Adamo, R. Cammi, J. W. Ochterski, R. L. Martin, K. Morokuma, O. Farkas, J. B. Foresman and D. J. Fox, *Gaussian 16, Revision B.01*, Gaussian, Inc., Wallingford CT, 2016.
56 V. S. Bryantsev, M. Blanco and F. Faglioni, *J. Phys. Chem. A*, 2010, **114**, 8165–8169.
57 M. W. Chase, Jr., *NIST-JANAF thermochemical tables*, 4th edn, Washington, DC: American Chemical Society; New York: American Institute of Physics for the National Institute of Standards and Technology, 1998.
58 P. D. C. Dietzel, R. K. Kremer and M. Jansen, *J. Am. Chem. Soc.*, 2004, **126**, 4689–4696.
59 J. M. Aubry, J. Rigaudy, C. Ferradini and J. Pucheault, *J. Am. Chem. Soc.*, 1981, **103**, 4965–4966.
60 E. J. Nanni, R. R. Birge, L. M. Hubbard, M. M. Morrison and D. T. Sawyer, *Inorg. Chem.*, 1981, **20**, 737–741.
61 M. Hayyan, M. A. Hashim and I. M. AlNashef, *Chem. Rev.*, 2016, **116**, 3029–3085.
62 H.-D. Lim, B. Lee, Y. Bae, H. Park, Y. Ko, H. Kim, J. Kim and K. Kang, *Chem. Soc. Rev.*, 2017, **46**, 2873–2888.
63 D. Sharon, D. Hirsberg, M. Salama, M. Afri, A. A. Frimer, M. Noked, W. Kwak, Y.-K. Sun and D. Aurbach, *ACS Appl. Mater. Interfaces*, 2016, **8**, 5300–5307.
64 D. G. Kwabi, M. Tułodziecki, N. Pour, D. M. Itkis, C. V. Thompson and Y. Shao-Horn, *J. Phys. Chem. Lett.*, 2016, **7**, 1204–1212.
65 Y. Wang and Y.-C. Lu, *Angew. Chem., Int. Ed.*, 2019, **58**, 6962–6966.
66 Y. Wang, Z. Liang, Q. Zou, G. Cong and Y.-C. Lu, *J. Phys. Chem. C*, 2016, **120**, 6459–6466.
67 D. G. Kwabi, T. P. Batcho, S. Feng, L. Giordano, C. V. Thompson and Y. Shao-Horn, *Phys. Chem. Chem. Phys.*, 2016, **18**, 24944–24953.
68 S. A. Freunberger, *Nat. Energy*, 2017, **2**, 17091.

